AGU PUBLICATIONS

JGR

Journal of Geophysical Research: Atmospheres

RESEARCH ARTICLE
10.1002/2014JD021617

Key Points:
- OH Meinel (5-1), (8-3), and (9-4) band VER profiles derived from OSIRIS observations
- Climatology shows OH emissions from higher vibrational levels peak at higher altitudes
- Not knowing OH emission profile can bias ground-based temperature measurements

Correspondence to:
P. E. Sheese,
psheese@atmosp.physics.utoronto.ca

Citation:
Sheese, P. E., E. J. Llewellyn, R. L. Gattinger, and K. Strong (2014), OH Meinel band nightglow profiles from OSIRIS observations, *J. Geophys. Res. Atmos.*, *119*, 11,417–11,428, doi:10.1002/2014JD021617.

Received 6 FEB 2014
Accepted 2 SEP 2014
Accepted article online 4 SEP 2014
Published online 3 OCT 2014

OH Meinel band nightglow profiles from OSIRIS observations

P. E. Sheese[1,2], E. J. Llewellyn[1], R. L. Gattinger[1], and K. Strong[2]

[1]ISAS, Department of Physics and Engineering Physics, University of Saskatchewan, Saskatoon, Saskatchewan, Canada, [2]Department of Physics, University of Toronto, Toronto, Ontario, Canada

Abstract The mesospheric nightglow spectrum is replete with OH Meinel band emissions, from the midvisible to the midinfrared. These emissions provide a wealth of aeronomic information, giving a physical view of the chemistry and dynamics of the upper atmosphere. The Optical Spectrograph and Infrared Imaging System (OSIRIS) instrument, on the Odin satellite, is currently one of the few satellite instruments that simultaneously observes emissions from multiple and separate Meinel bands. This has allowed the derivation of near-global data sets of nighttime OH volume emission rate profiles for the Meinel (5-1), (8-3), and (9-4) bands. The 2002–2013 climatologies consistently show that emission from bands in higher upper vibrational levels peaks at higher altitudes. The global average (5-1), (8-3), and (9-4) band emission peak heights are at altitudes of 86.0 km, 86.7 km, and 87.1 km, respectively. The 1σ variation in the (5-1), (8-3), and (9-4) band, peak heights are 1.8 km, 1.9 km, and 1.9 km, respectively. The climatological (30 day, 10° latitude) peak heights can vary significantly with both time and latitude; however, the (5-1) band climatological peak height is nearly always below that of the (8-3) band, which is nearly always below that of the (9-4) band. The temporal variation in the emission peak height can have a significant impact on measurements of OH rotational temperatures from ground-based observations of the OH layer. It was found that omitting the profile climatology can bias a ground-based temperature measurement by as much as ±4 K and can also make ground-based measurements susceptible to nonrealistic temperature variations.

1. Introduction

Observations of the mesospheric visible-infrared nightglow emission spectrum are replete with the OH Meinel bands—named after Aden Meinel, who first identified the emissions [*Meinel*, 1950]. These emission features are spectrally widespread, as excited OH is formed in the upper vibrational levels through the reaction

$$H + O_3 \rightarrow OH*(v \leq 9) + O_2 \quad (1)$$

The vibrationally excited OH can deactivate through spontaneous emission, and the change in vibrational levels in this process can be in the range of $\Delta v = 1$ to $\Delta v = 9$. For instance, the Meinel (6-0) band is centered near 530 nm, whereas the (9-8) band is in the infrared near 4.5 μm. Excited OH molecules can also be quenched through a collision with O, O_2, and N_2, although exactly how OH is collisionally deactivated has been an issue of contention since *McDade and Llewellyn* [1987] first proposed that such quenching could occur into a lower vibrational level where $\Delta v > 1$ (multiquantum vibrational deactivation). *Evans and Llewellyn* [1972] had previously suggested that $\Delta v = 1$ quenching was dominant.

This study reports on the climatology of the OH (8-3), (9-4), and (5-1) emission profiles, derived from OSIRIS (Optical Spectrograph and Infrared Imaging System [*Llewellyn et al.*, 2004] on the Odin satellite [*Murtagh et al.*, 2002]) measurements of the OH nightglow emissions. These bands were chosen as they are fully within the OSIRIS spectral range and have the highest signal-to-noise ratios of all Meinel bands that OSIRIS can observe. The study focuses on the differences in peak heights between Meinel bands with different upper vibrational levels. In addition, it is shown that departures from the average OH emission profile at any given time/location can affect ground-based measurements of mesospheric temperatures if the variations in the emission profiles are not properly taken into account. This topic has been discussed previously in a number of studies, e.g., *Takahashi et al.* [2005], *Liu and Shepherd* [2006], *Mulligan et al.* [2009], and *von Savigny et al.* [2012].

The idea that the Meinel band emission peaks at different altitudes depending on the upper vibrational level (v') has been explored in some previous studies. At first, measurements of the differences in volume

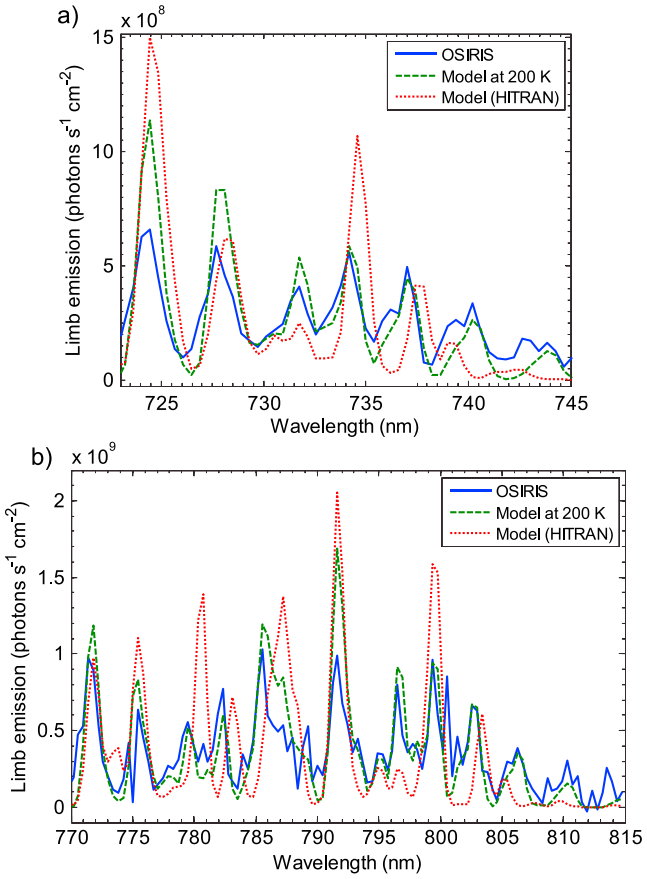

Figure 1. Average OSIRIS limb emission measurements between 70 and 100 km for one orbit on 6 August 2003 and spectra at 200 K from two different models. (a) OH (8-3) band emission. (b) OH (9-4) and (5-1) band emissions.

emission rate (VER) peak heights were attempted through the use of rocket-borne instruments, e.g., *Rogers et al*. [1973], *Evans et al*. [1973], *López-Moreno et al*. [1987], and *McDade et al*. [1987]. *Baker and Stair* [1988] have compiled a more complete list of previous rocket studies that examined the OH emission in different Meinel bands, while *Mende et al*. [1993] attempted to measure the emission peak height differences using observations from the Space Shuttle. More recently, near-global coverage of Meinel emissions has been possible through the use of satellite-based instruments, e.g., Wind Imaging Interferometer (on the UARS satellite), SABER (Sounding of the Atmosphere using Broadband Emission Radiometry on the Thermosphere, Ionosphere, Mesosphere Energetics and Dynamics satellite), and SCIAMACHY (SCanning Imaging Absorption spectroMeter for Atmospheric CartograpHY on Envisat). *Kaufmann et al*. [2008] and *von Savigny et al*. [2012] have both discussed the OH limb peak height variation with v' in terms of SCIAMACHY observations and suggest that there is indeed a peak height difference between emissions with different v'. *von Savigny and Lednyts'kyy* [2013] expand on this topic and discuss the role atomic oxygen plays in separating Meinel band peak heights.

In this study, the OSIRIS instrument and the method used to determine the OH VER profiles are discussed in section 2. The resulting peak height climatologies and their impact on ground-based mesospheric temperature retrievals are discussed in section 3, and the results are summarized in section 4.

2. The Determination of the OH Emission Profiles

The OH VER profiles were derived from OSIRIS limb radiance observations. The Odin satellite, which includes OSIRIS, was launched in 2001 into a Sun-synchronous orbit with a nominal ascending/descending node of 18:00/06:00 LT. The OSIRIS instrument [*Llewellyn et al*., 2004] has a 1 km vertical field of view and scans the Earth's limb between ~7 and 110 km, with a pointing knowledge of ~0.5 km. The OSIRIS spectrograph observes airglow and scattered sunlight over the spectral range from the near UV to the near IR, 275–810 nm, with approximately 1 nm spectral resolution. The spectrograph signal is detected using a CCD detector with 1353 pixels that span the spectral range, approximately 0.4 nm/pixel. The absolute calibration uncertainty is estimated to be within ±10%, and the precision is within 5%. Spectral measurements of nighttime airglow emissions are not expected to suffer from nonlinearities due to stray off-axis light nor due to the instrument response to polarized light. Averaged OSIRIS limb-column radiances between tangent altitudes of 70 and 100 km for one orbit on 6 August 2003 are shown in Figure 1. Modeled VER spectra, using two different models (discussed below), at 200 K are also shown.

The retrieval method derives the OH spectral profiles at each pixel in the wavelength region of 722.8–745.1 nm for the (8-3) band and 769.8–814.8 nm for the (9-4) and (5-1) bands; comprising 168 pixels in total. In addition, all three methods interpolated the OSIRIS observations on to a 1 km altitude grid; and for each line of sight along the grid, geometric path lengths through the atmosphere separated into 1 km concentric shells were calculated for the inversion (hereinbelow, the matrix of path lengths will be known as **K**). VER spectra were retrieved at altitudes from 60 km up to the top altitude of each individual OSIRIS scan—typically between 100 and 110 km, but never below 97 km.

The retrieval method was derived from a regularized least squares approach. This is a statistical weighting approach that uses the measurement covariance matrix and a "regularization" matrix as statistical weights. For any given pixel *p*,

$$\hat{x}_p = \left(\mathbf{K}_p^T \mathbf{S}_p^{-1} \mathbf{K}_p + \gamma \mathbf{L}^T \mathbf{L}\right)^{-1} \mathbf{K}_p^T S_p^{-1} y_p, \tag{2}$$

where $\hat{x}_p$ is the VER solution profile, $\mathbf{y}_p$ is the OSIRIS radiance profile, $\mathbf{S}_p$ is the associated OSIRIS measurement covariance matrix, $\mathbf{K}_p$ is the weighting function matrix (the geometric path lengths), **L** is the regularization matrix, and γ is a scale factor that was iteratively chosen to minimize the cost function

$$\chi^2 = \sum_{i=1}^{N} \left(\sum_{j=1}^{M} K_{ij}\, x_j - y_i \right)^2 - \sum_{i=1}^{N} \sigma_i^2, \tag{3}$$

where *N* is the number of lines of sight in an OSIRIS scan, *M* is the number of assumed concentric shells in the atmosphere (in every case *M* was chosen to equal *N*), and σ_i^2 are the diagonal elements of $\mathbf{S}_p$ [*Eriksson*, 2000]. When the cost function is minimized, the sum of the squared differences between the measurement and the forward model is as close as possible to the sum of the squared measurement errors. A vertical smoothing matrix of the form of equation (6.33) given by *Rodgers* [2008] was chosen for the regularization matrix **L** in order to dampen unrealistic oscillations in the retrieved VER profile. One advantage of this approach is that an approximation of the uncertainty due to instrument noise and to smoothing is relatively straightforward. Equation (4) is used for the retrieval contribution function matrix

$$\frac{\partial \hat{\mathbf{x}}}{\partial \mathbf{y}} = \mathbf{G} = \left(\mathbf{K}^T \mathbf{S}^{-1} \mathbf{K} + \gamma \mathbf{L}^T \mathbf{L}\right)^{-1} \mathbf{K}^T \mathbf{S}^{-1}. \tag{4}$$

The error in the retrieval due to instrument noise is then $\mathbf{G}\boldsymbol{\sigma}$, where $\boldsymbol{\sigma}$ is the instrument noise vector, and the smoothing error can be approximated as $\mathbf{GK}\hat{\mathbf{x}}$. The sum of these two terms is referred to as the retrieval uncertainty. The retrieval uncertainty in the (8-3) band is typically within 25–100 photons s^{-1} cm^{-3}, and in the (9-4) and (5-1) bands it is typically within 50–150 photons s^{-1} cm^{-3}. The typical uncertainty profile peaks with the VER profile peak, and the measurement vertical resolution is typically on the order of 1.5–2 km.

An example of the difference between the derived (8-3) band VER profiles for the three different retrieval methods, together with the retrieval uncertainty in the regularized retrieval, is shown in Figure 2a. The column (60–104 km) VER spectra derived from the three different methods for the same OSIRIS scan as Figure 2a are shown in Figure 2b. There are clear differences between the VER profiles, especially in the region where the VER is on the same order as the retrieval uncertainty. However, the difference in the retrieved total column VER is almost nonexistent, implying that errors incurred due to the different techniques are averaged out over the profile. A modeled (8-3) band VER spectrum (model discussed below) at 200 K is also shown in Figure 2b.

The derivations of the (9-4) and (5-1) band profiles are somewhat more complicated as their spectra overlap, and so the derivations of the total (9-4) and (5-1) VER profiles require model OH Meinel band spectra. For each band, the model calculated the relative rotational line strengths using the formulae for doublet transitions given by *Kovács* [1969]. Only rotational lines for $K \leq 20$ were simulated in the model, and the spectra were convolved with the OSIRIS slit function, which has a full width at half maximum of 0.95 nm. Model spectra of the (9-4) and (5-1) line intensities at a temperature of 200 K are shown in Figure 3a, together with the total spectrum. Figure 3b shows the relative contribution from the separate (9-4) and (5-1) bands to the total modeled convolved spectrum. These contributions were used as weights in summing the emission rates in the (9-4) and (5-1) spectral region in order to derive the separate (9-4) and (5-1) total band intensities. Figure 1b also shows a modeled spectrum at 200 K that used HITRAN 2012 [*Rothman et al.*, 2013] OH line strengths and positions in the (9-4) and (5-1) bands, instead of calculated values. It can be seen that the model using the HITRAN parameters led to a poorer fit with the OSIRIS data.

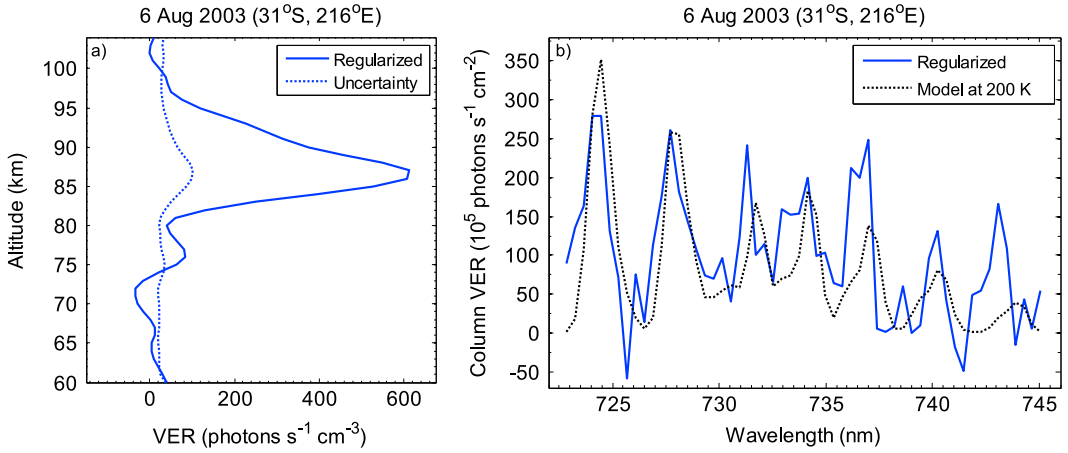

Figure 2. Example of a OH (8-3) band VER retrieval. (a) A derived-VER profile for an OSIRIS scan on 6 August 2003 (31°S, 216°E), and the retrieval uncertainty in the (b) retrieved column VER spectrum for the same scan and a modeled emission spectrum at 200 K.

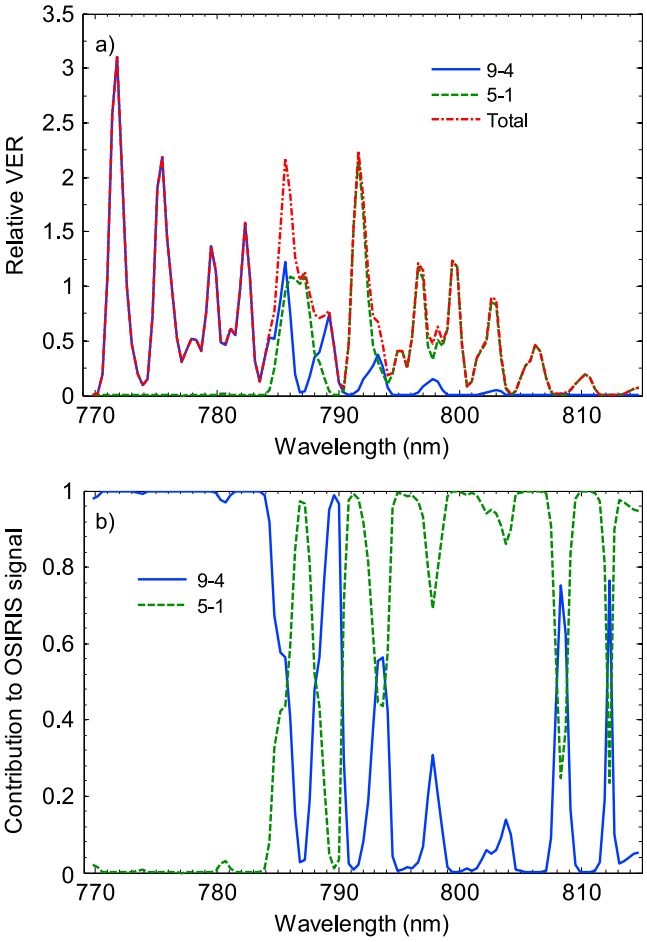

Figure 3. (a) Model spectra of OH (9-4) and (5-1) band VER at 200 K convolved with the OSIRIS slit function. (b) Weighting functions for the contributions of the (9-4) and (5-1) bands to the total retrieved VER spectrum.

3. Peak Height Climatology

In the following sections, in order to avoid observations with solar signal contamination, all data were derived for locations where the solar zenith angle was greater than 103°. Also, in order to keep the local time of the data consistent, only PM data were used. This corresponds to local times of ~18:30 at low latitude and midlatitude regions, and closer to midnight near the poles. All data have been screened for anomalous values (outliers due to retrieval error or possible highly energetic particles) and, in the near-polar regions, for possible auroral contamination. In the (8-3) band, any profiles that had total band VER values outside ±1000 photons s^{-1} cm^{-3} were omitted. In the (9-4) and (5-1) bands, any profiles that had total band VER values outside ±1500 photons s^{-1} cm^{-3} were omitted. These criteria led to the exclusion of 2.7% of the VER profiles. Negative VER values were not omitted so as to avoid skewing the mean. Observations of the N_2^+ first negative (0-0) line at 391.4 nm were used to determine if there was any detectable aurora within the OSIRIS line of sight. The N_2^+ first negative (0-0) line is the strongest auroral signature

detected by the OSIRIS instrument, apart from the O_2 A band and the atomic oxygen green line [*Gattinger et al.*, 2010]. If two or more tangent altitudes in a scan had an observed radiance greater than the OSIRIS noise threshold at 391.4 nm, it was concluded that there was a possibility of auroral contamination within the scan and the OH VER profile was not retrieved.

3.1. The Altitude of the Meinel Band Emission Peak

It is generally accepted that OH Meinel band VER profiles have a peak near ~87 km, with a full width at half maximum (FWHM) of ~8 km. Although, as previously mentioned, there are some studies that show that an emission profile from OH molecules in a higher upper vibrational level (v') will, generally, have a higher-peak height. In a recent study, *von Savigny et al.* [2012] included an excellent review on this topic and summarized the findings of past models and experiments [e.g., *Baker and Stair*, 1988], as well as presenting their own model and experimental results. *von Savigny et al.* [2012] also found, from an analysis of SCIAMACHY limb radiances in the OH (3-1), (6-2), and (8-3) bands, that the separation in peak height between upper vibrational levels was on the order of 0.5 km for $\Delta v = 1$. The model results of *von Savigny et al.* [2012] (based on the model of *McDade* [1991], with multiquantum relaxational O_2 quenching) were found to be consistent with the measured results, and "the SCIAMACHY observations [were] consistent with the majority of the previously published results" [*von Savigny et al.*, 2012].

Examples of (8-3), (9-4), and (5-1) VER profiles retrieved from the OSIRIS observations are shown in Figures 4a and 4b. The three band profiles shown in Figure 4a are for an OSIRIS scan on 6 May 2008, near (66°S, 118°E); and those in Figure 4b are for 9 January 2009, near (57°S, 281°E). In the first (6 May) case, the (5-1) band peaks near 90 km, the (8-3) band peaks near 89–90 km, and the (9-4) band peaks near 88–89 km. Given the associated uncertainty in the VER profiles and the OSIRIS vertical field of view of ~1 km, it is impossible to determine that any band's profile peak height is above that of any others. The error bars in Figures 4a and 4b indicate the uncertainty at the peak heights on a 1 km grid. In the second (9 January) case, all three bands peak near 85 km. It should be noted, that it is not difficult to find scans within the data set where the (5-1) profile has the highest peak or where the (9-4) profile has the lowest peak.

If we look at all the VER profiles in the orbits associated with these two scans (Figures 4c and 4d), we see that the peak height is highly variable from location to location. In the orbit on 6 May 2008, the VER peak height for all three bands vary quite closely together between approximately 82 and 90 km depending on the latitude; although the average (5-1) peak height is lower than that of the other two bands. Less peak height variation is exhibited in the 9 January 2009 orbit, in the range of ~84–89 km; but again, the average (5-1) peak height is lower than that of the other two bands.

Nothing conclusive about the distributions of peak heights can be gleaned from looking at a single scan or a single orbit, except that they are highly variable. But, if we look at the OSIRIS climatology for those two orbits, Figures 4e and 4f, a clearer picture is formed. Figure 4e represents the mean of all OSIRIS data for 6 May ± 15 days from 2003–2012 (zonal mean), and in latitude the data have been smoothed by the 7° running mean (representing the minimal separation between OSIRIS scans). The same is true in Figure 4f but for 9 January. In both cases there is a clear separation of peak height between the different bands. In the 6 May climatology, the low latitude and midlatitude tend to exhibit slightly higher OH peak heights than in the high or equatorial latitudes; however, the (9-4) VER profiles consistently peak at higher altitudes than the (8-3) band (an average of 0.55 km higher), and the (8-3) VER profiles consistently peak at higher altitudes than the (5-1) band (an average of 0.67 km higher). In the 9 January climatology, again, the (9-4) VER profiles consistently peak at higher altitudes than the (8-3) band (an average of 0.54 km higher), and the (8-3) VER profiles consistently peak at higher altitudes than the (5-1) band (an average of 0.60 km higher).

Similar peak height climatologies were constructed for all three bands at all latitudes and days of the year from 2002 to 2013. In Figures 5a–5c, the (5-1), (8-3), and (9-4) climatologies, smoothed in time by the 30 day running mean and smoothed in latitude by the 10° running mean, are shown. These peak heights are mostly consistent with the 2002 SABER values shown in *Baker et al.* [2007]. The SABER data, like the OSIRIS data, exhibit a semiannual oscillation in peak height in the northern and southern low latitudes, with higher-peak heights near solstice and lower near equinox. As well, both the SABER and OSIRIS data exhibit lower peak heights in the midlatitude and high latitude regions near solstice, with higher-peak heights near equinox. There is less agreement between the OSIRIS and the SABER data in the northern midlatitudes.

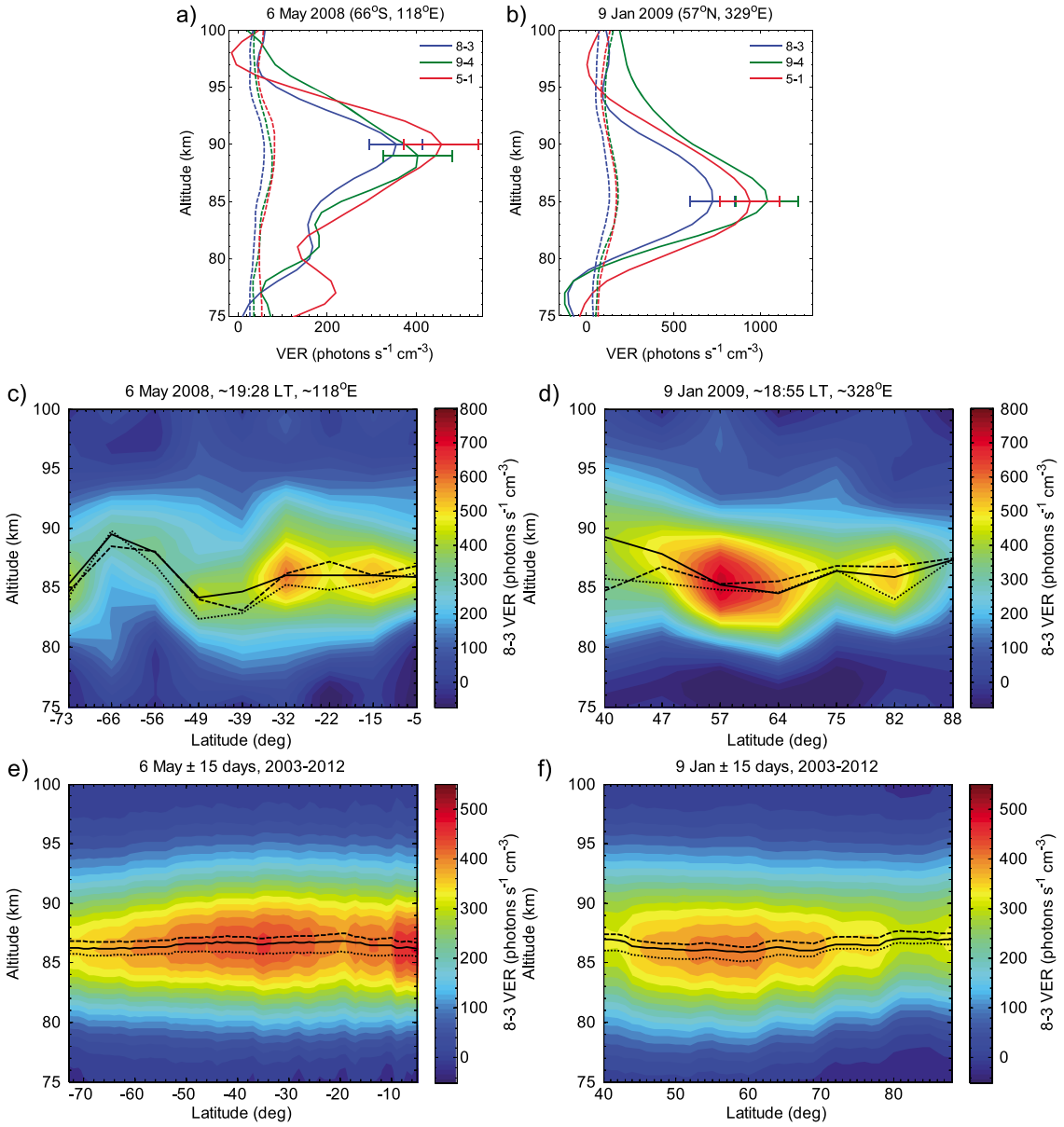

Figure 4. (a and b) Retrieved OH VER profiles (solid lines) and corresponding retrieval uncertainty (dashed lines) for two separate OSIRIS scans. (c and d) Retrieved VER profiles for the ascending (PM) phase of two OSIRIS orbits. (e and f) OSIRIS VER climatology for times/locations in Figures 4c and 4d. Note that the contour plots are not all on the same color scale. In Figures 4c–4f, the solid lines indicate the (8-3) peak heights, the dashed lines indicate the (9-4) peak heights, and the dotted lines indicate the (5-1) peak heights.

For the overwhelming majority of locations, the OSIRIS (5-1) emission peaks at lower altitudes than the other two bands, and the (9-4) emission peaks at higher altitudes. The climatological peak heights of all three bands, as shown in Figure 5, are highly correlated with each other. Comparing the different bands' climatological peak heights, the correlation coefficient is 0.91 between the (9-4) and (8-3) bands, 0.88 between the (9-4) and (5-1) bands, and 0.87 between the (8-3) and (5-1) bands. However, the peak height correlation coefficients for the unsmoothed data are 0.64, 0.60, and 0.58, respectively. The lower correlation values are due to the noise associated with individual scans.

The average (9-4) peak height is 87.1 km, the average (8-3) peak height is 86.7 km, and the average (5-1) peak height is 86.0 km. The average (9-4) FWHM is 11.1 km, the average (8-3) FWHM is 10.4 km, and the average (5-1) FWHM is 8.2 km. The climatologies of the corresponding peak height variations

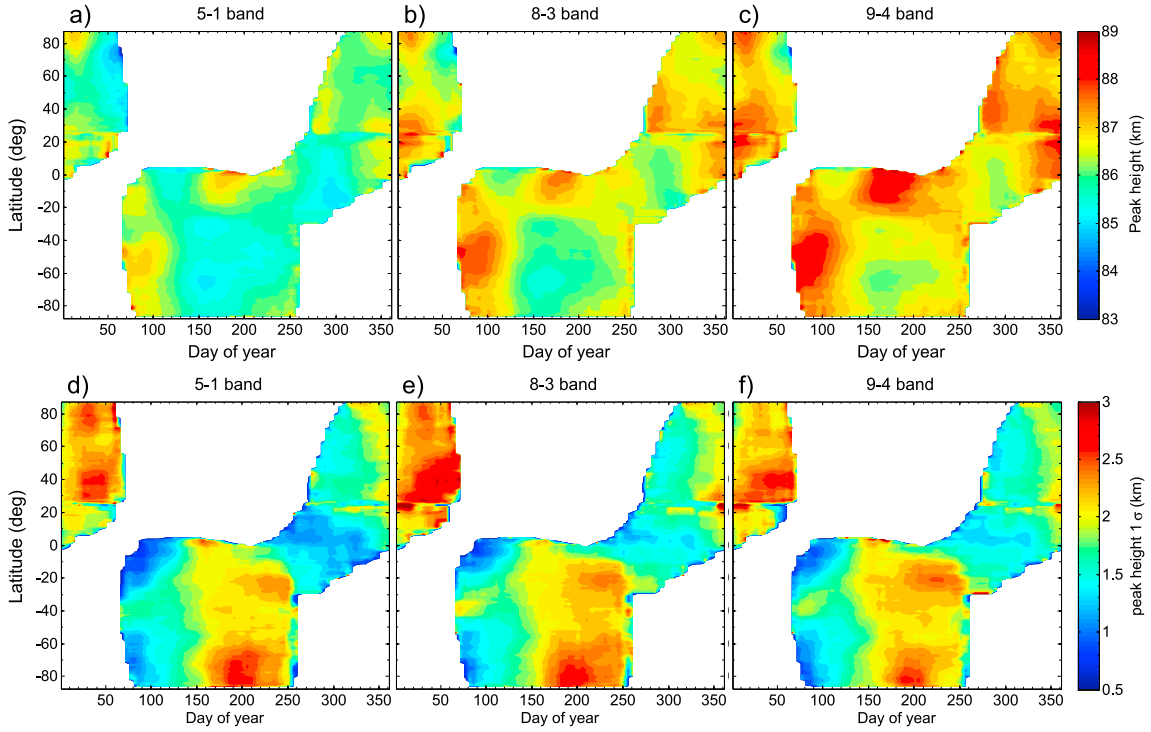

Figure 5. (a–c) OH VER peak height climatologies and (d–f) corresponding 1σ standard deviation. All data have been smoothed in time by the 30 day running mean and in latitude by the 10° running mean.

(1σ deviations), shown in Figures 5d–5f, are very similar to one another and typically range from ~1 to 3 km, depending on the day and latitude. Both the (9-4) and (8-3) climatological peak height variations are 1.9 km, and the (5-1) average variation is 1.8 km. When random error, on the order of the measurement error, is added to the data, the average 1σ (500 trials) change in peak height is ~0.14 km for all three bands. Therefore, the observed variations predominantly represent the natural variation, not noise due to measurement error. The model used for the (9-4) and (5-1) band weights also introduces systematic uncertainty in the peak height measurements of those bands. Changing the relative (9-4) to (5-1) band strength by 20% shifts the mean (9-4) peak height by 0.03 km and the mean (5-1) peak height by 0.01 km. If weights based on HITRAN 2012 line parameters are used, the peak heights are shifted by 0.06 km and 0.34 km, respectively. However, as shown in Figure 1, the HITRAN values lead to significantly worse fits to the OSIRIS measurements.

Figure 6a shows the differences between the (9-4) and (8-3) climatological peak heights. Figure 6b shows the same as Figure 6a but between the (8-3) and (5-1) bands. The mean difference between the (9-4) and (8-3) bands is 0.46 ± 0.24 km, and the mean difference between the (8-3) and (5-1) bands is 0.66 ± 0.29 km. If the two height-difference climatologies are combined, and the separation of OH emission peak heights as a function of v' is assumed to be linear, the separation is 0.34 ± 0.22 km per upper vibrational level—consistent with, although somewhat smaller than, the findings of *von Savigny et al.* [2012], ~0.5 km per upper vibrational level. It should be noted that even though the measurement resolution is on the order of 2 km, with a pointing knowledge of 0.5 km, since the OSIRIS altitude registration is not wavelength dependent, and OSIRIS observations are not on a constant vertical grid, an average peak height separation on the order of 0.5 km can be determined when averaging thousands of profiles.

However, the two height-difference climatologies are moderately anticorrelated, with a correlation coefficient of −0.49. This suggests that the separation in peak height is not a linear function of v', but rather varies with the local dynamics and chemistry; this conclusion is only partially consistent with the model results of *von Savigny et al.* [2012]. In those model simulations, the emission peak height was not a linear function of v'; although, unlike the OSIRIS observations, the model simulations suggested that peak

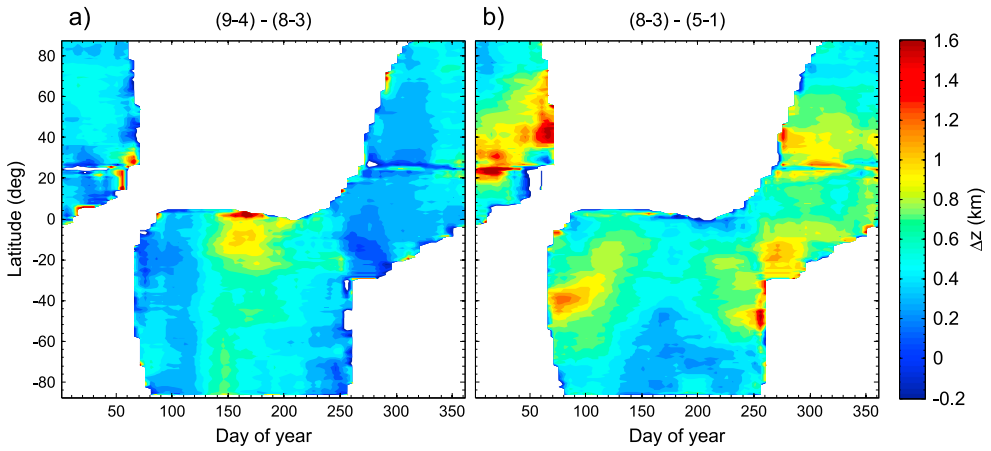

Figure 6. Differences in climatological peak heights between (a) the (9-4) and (8-3) bands, and (b) the (8-3) and (5-1) bands. All data smoothed by 30 day running mean and 10° running mean.

heights are more narrowly spaced between emissions with higher values of v' and more widely spaced between lower v' emissions. As discussed by *von Savigny et al.* [2012], the model results at lower v' values also are not entirely in agreement with the SCIAMACHY observations, and this could be due in part to uncertainties in the atomic oxygen density profile and in the O and O_2 quenching coefficients used in their model.

3.2. Impact of Height Profile Variation on Ground-Based Measurements

As noted above, the height at which OH emissions peak is quite variable through time and latitude. In addition, emissions from different upper vibrational levels peak at different altitudes. These findings can have a significant impact on ground-based measurements of mesospheric temperatures derived from Meinel band observations used to study gravity waves. To investigate the possible impact on ground-based OH temperature retrievals, we use a simple model to simulate ground-based temperatures for three different cases, for a given temperature profile time series. In each of the three cases, emission spectra are modeled at each time step, 1 day, based on an assumed temperature profile and OH emission profile. For each day, the spectra are vertically integrated between 70 and 104 km, in order to simulate a zenith-looking ground-based measurement. The integrated spectra are then fit to modeled temperature dependent spectra to simulate ground-based OH temperatures. The "derived" case assumes a variable OH emission profile—OSIRIS band intensity measurements. The "seasonal mean" case assumes a constant OH emission profile corresponding to the mean OSIRIS emission profile for the region being investigated. And the "fixed" case assumes a constant OH emission profile, a Gaussian distribution peaking at 87 km, with a FWHM of 8 km. It should be noted that the OSIRIS spectral measurements are not being used to derive actual OH rotational temperatures. The purpose here is not to validate OH rotational temperatures but to examine how ground-based OH temperatures can be affected by changes in the OH emission layer.

The derived case is the best estimate of the temperature, a ground-based instrument would derive if it was observing the assumed atmosphere in the zenith, and the OH layer varied as measured by OSIRIS. The seasonal mean case that gives the temperature a ground-based instrument would derive if the OH layer remained constant, corresponding to the local mean OSIRIS measurements. The fixed case gives the ground-based temperature if the OH layer was a fixed Gaussian peaking at 87 km with a FWHM of 8 km.

The first region tested was in the Arctic (northward of 65°N) during the 2008/2009 winter season. This was chosen as a special phenomenon that was observed at this time—a sudden stratospheric warming, which had a significant effect in the upper atmosphere. Figure 7a shows a profile time series of the Arctic average (8-3) band VER, smoothed by the 3 day running mean. The black solid line indicates the peak height, and the black-dotted lines indicate the half maxima. The peak height and half maximum time series are also superimposed in Figure 7b, a plot of simultaneously derived OSIRIS O_2 A-band temperatures

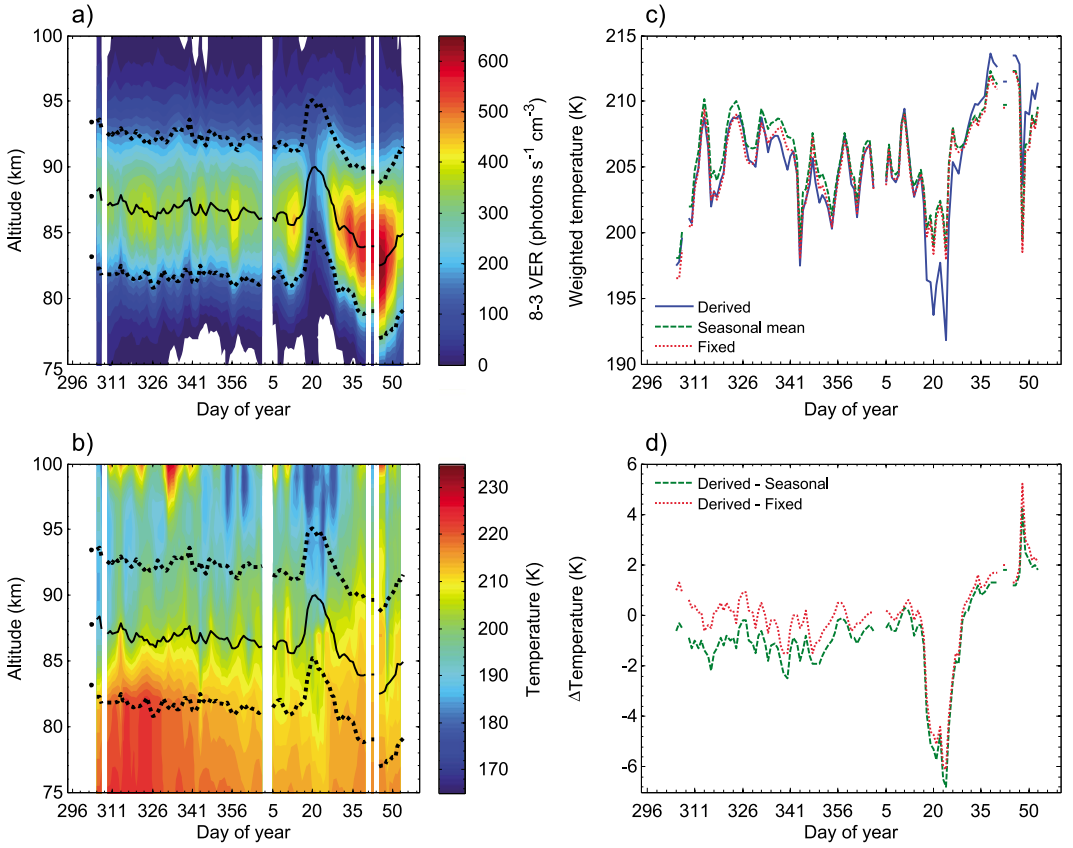

Figure 7. (a) OSIRIS derived OH (8-3) VER profiles for Arctic 2008/2009 winter, smoothed by the 3 day running mean. (b) Corresponding OSIRIS O_2 A-band temperatures (smoothed to MSIS temperatures below 85 km). (c) Time series of height-averaged temperatures, weighted differently for the derived, seasonal mean, and fixed cases (see text). (d) Height-averaged temperature differences between the derived and seasonal mean cases and between the derived and fixed cases. In Figures 7a and 7b, the solid lines indicate the (8-3) emission peak heights, and the dashed lines indicate the emission layer half widths.

[*Sheese et al.*, 2010], also smoothed by the 3 day running mean. Note that these are not OH rotational temperatures. Since the A-band temperature retrievals are limited to altitudes above 85 km, below 85 km the temperature profiles are smoothed to corresponding NRL-MSISE-00 temperatures [*Picone et al.*, 2002]. Although there was an obvious variability in the peak height throughout the selected period, the seasonal mean peak height for this region was 86.4 km, and the seasonal mean FWHM was 11.2 km. Figure 7c shows the simulated temperatures for the three different cases, and Figure 7d shows the difference between the derived and seasonal mean cases and the difference between the derived and fixed cases. These results show that even in the case where the seasonal mean profile is known, the forward modeled column temperature can be in error by approximately 2 K. In the extreme case, when there was an extreme rise in altitude of the emitting layer, along with a cooling of the mesopause region, the absolute difference was slightly less than 7 K.

The same procedure was applied for a region not affected by any special phenomena, the 2010 autumn/winter in the latitude range of 30–60°S. Figures 8a–8d are the same as Figures 7a–7d, except for the conditions of this new region, and daily Mass Spectrometer Incoherent Scatter (MSIS) temperatures at 18:00 UT and (45°S, 0°E) are used instead of derived and smoothed OSIRIS temperatures. The seasonal mean (8-3) peak height was 86.7 km with a mean FWHM of 10.7 km. For both the seasonal mean and fixed cases, the forward modeled temperatures can differ from the derived case by approximately ±2 K. This suggests that, without an accurate knowledge of the OH VER profile, ground-based measurements of temperature profiles would have approximately a ±2 K uncertainty, before taking into account

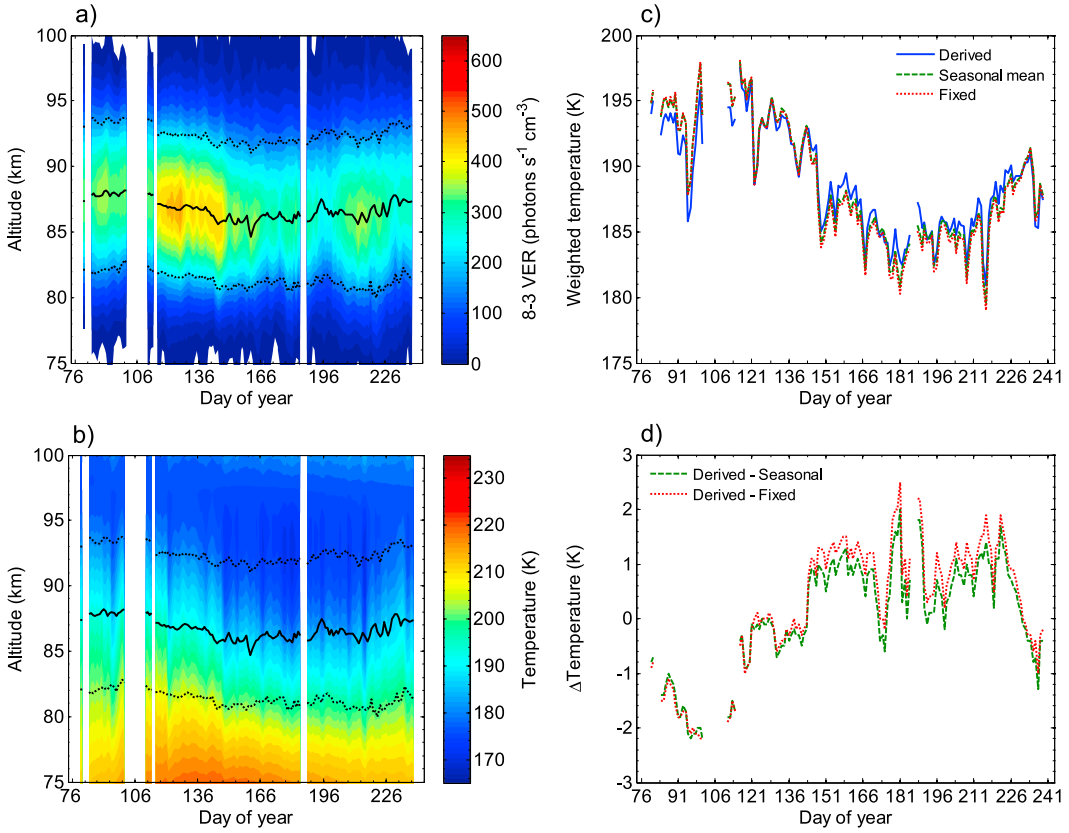

Figure 8. Same as Figure 7 but for the 2010 autumn/winter in the southern midlatitudes, and temperatures in Figure 8b are daily MSIS temperatures at 18:00 UT and (45°S, 0°E).

instrument noise or any systematic uncertainties. In addition, ground-based OH temperatures would be more subject to variability than an instrument that was sensitive to a constant altitude regime.

The ±2 K variation described above may not seem significant, however that was using the (8-3) band, which does tend to peak near 87 km. If a constant peak height is assumed, the magnitude of temperature uncertainty due to the peak height is dependent on v' of the observed emission band. For instance, if a peak height of 87 km is assumed, it is likely that ground-based retrievals from observations in the (3-1) band will be further from the true 87 km temperature than similar retrievals from the (8-3) band. This is exemplified in Figure 9, which shows OSIRIS 2011 time series within the Antarctic (south of 65°S), using the same three cases as above but using the (9-4), (8-3), and (5-1) bands. Here daily temperatures were taken from MSIS at 18:00 UT and (75°S, 0°E). It should be noted that the (5-1) band is not typically used in ground-based observations, but bands with a lower v' are frequently used, such as the (3-1) band. Figure 9a shows the daily MSIS temperatures, with the peak heights of the OSIRIS (9-4), (8-3), and (5-1) bands superimposed. Again, the (9-4) band exhibits the highest peak heights and the (5-1) band exhibits the lowest. Figure 9b shows the derived case temperature minus the fixed case temperature for all three bands. On short time scales, all three bands show temperature variations on the order of 2 K, and these represent spurious variations in the derived temperatures due to vertical displacement of the OH emission layer. Overall, the offset between the derived temperatures and the fixed (~87 ± 4 km) temperatures can be on the order of 4 K, depending on the band. The temperature differences between the derived temperatures and the temperatures derived from the use of the individual bands' seasonal mean profiles are shown in Figure 9c. Again, in all three bands, temperature variations are on the order of 2 K; however, the offset is somewhat improved and in all three bands is typically less than 3 K. These results can help explain previously reported temperature differences between ground-based and satellite-based temperatures that can be up to 15 K [e.g., *Mulligan and Lowe*, 2008], as well as biases between the two methods that can be on the order of 2–10 K [e.g., *French and Mulligan*, 2010].

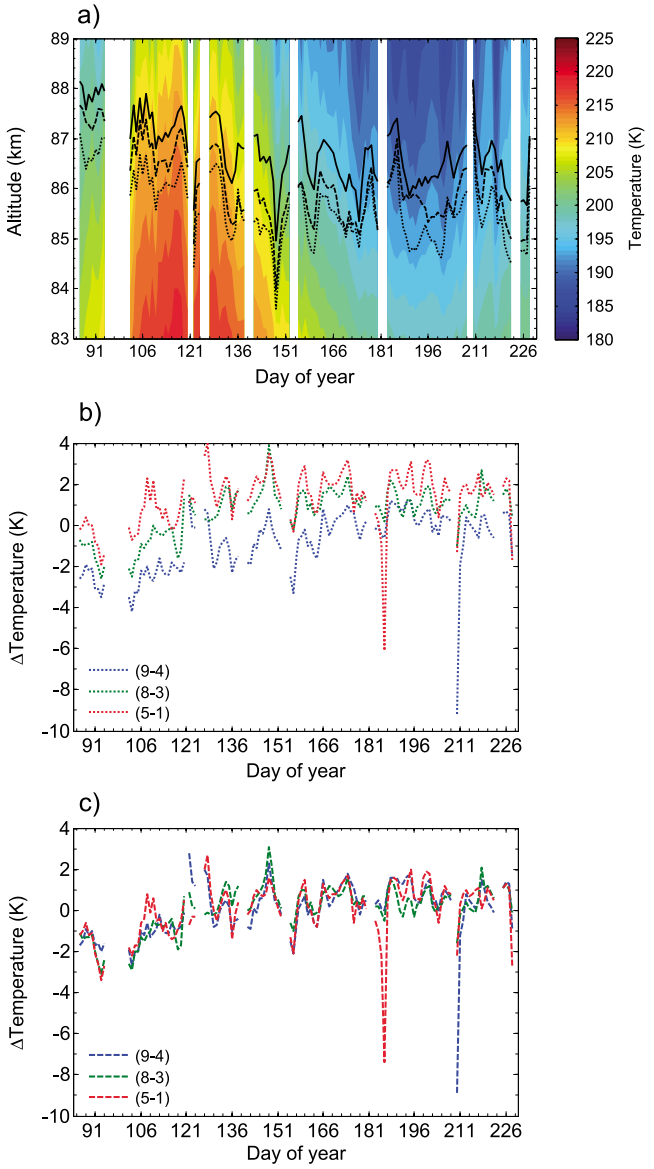

Figure 9. Time series in the 2011 Antarctic (south of 65°S) winter. (a) Daily MSIS temperatures at 18:00 UT and (75°S, 0°E), the solid, dashed, and dotted lines are the OSIRIS (9-4), (8-3), and (5-1) peak heights smoothed by the running 3 day mean. (b) Temperature differences between the derived and fixed cases (derived-fixed). (c) Temperature differences between the derived and seasonal mean cases (derived-seasonal).

4. Summary and Discussion

OSIRIS limb radiance observations have been used to retrieve nighttime OH VER profiles in the (5-1), (8-3), and (9-4) Meinel bands. The OSIRIS data set currently spans July 2002 through March 2013, in an altitude region of 60 to ~105 km.

The peak heights of the three different bands can vary significantly, between ~82 and 92 km, in both time and latitude. Even within a single OSIRIS orbit, peak heights can be seen to deviate far from the climatological mean. When observing the VER profiles of a single OSIRIS scan, the level of retrieval uncertainty within the data (typically on the order of 50-100 photons s^{-1} cm^{-3}) and the 1 km OSIRIS field of view are often too large to determine which band peaks at the highest altitude and which at the lowest. However, the separation of climatological peak heights as a function of upper vibrational level is quite consistent. On average, the (5-1) band emission peaks at an altitude of 86.0 km with a standard deviation of 1.8 km, the average (8-3) peak height is at 86.7 km with a standard deviation of 1.9 km, and the average (9-4) peak height is at 87.1 km with a standard deviation of 1.9 km. The average peak heights are considered to be discernable since we are averaging over thousands of scans, and the OSIRIS altitude registration is not wavelength dependent.

If the separation between the peak heights of the Meinel bands is assumed to be a linear function of v', the OSIRIS data suggest a separation of 0.34 ± 0.22 km per upper vibrational level. This result is consistent with the model simulations of *von Savigny et al.* [2012]. However, the weak anticorrelation between the difference in (9-4) and (8-3) peak heights and the difference in (8-3) and (5-1) peak heights suggest that the separation is not linear with respect to v'.

The deviations in peak height and layer thickness from the assumed or climatological mean can have significant implications for monitoring mesospheric OH temperatures from the ground. Not taking the true band emission peak height into account can lead to temperature biases on the order of ±2–4 K, and up to ~7 K in extreme cases. The potential for higher biases is increased if the actual band peak height is further away from the assumed peak height—for instance, using a band with a lower v', e.g., the (3-1) band, under the assumption of an 87 km peak height. Not taking into account that the correct peak height over

time also has the potential to create specious variation in the ground-based data set, indicative of the change in sampling height, not in the temperature within a fixed altitude regime.

With this in mind, it is suggested that ground-based OH temperature retrievals should incorporate satellite (OSIRIS, SCIAMACHY, SABER, etc.) Meinel emission profile variations into their retrievals in order to avoid the sources of error outlined above. One simple method could be to ensure that temperatures and temperature variations do not significantly change when only using a subset of ground-based data that are coincident with satellite measurements. In cases where there is a significant change, ground-based temperatures could potentially be improved by taking into account the corresponding variations in climatological peak height/FWHM (from satellite data) and adjusting by the bias in the corresponding climatological satellite-based temperature profile.

Acknowledgments

This work was supported in part by the Natural Sciences and Engineering Research Council (Canada). Odin is a Swedish-led satellite project funded jointly by Sweden (SNSB), Canada (CSA), France (CNES), and Finland (Tekes), with support by the third party mission programme of the European Space Agency (ESA). All data are freely available by contacting the lead author.

References

Baker, D. J., and A. T. Stair Jr. (1988), Rocket measurements of the altitude distribution of the hydroxyl airglow, *Phys. Scr.*, *37*, 611–622, doi:10.1088/0031-8949/37/4/021.

Baker, D. J., B. K. Thurgood, W. K. Harrison, M. G. Mlynczak, and J. M. Russell (2007), Equatorial enhancement of the nighttime OH mesospheric infrared airglow, *Phys. Scr.*, *75*, 615–619, doi:10.1088/0031-8949/75/5/004.

Eriksson, P. (2000), Analysis and comparison of two linear regularization methods for passive atmospheric observations, *J. Geophys. Res.*, *105*, 18,157–18,167, doi:10.1029/2000JD900172.

Evans, W. F. J., and E. J. Llewellyn (1972), Excitation rates of the vibrational levels of hydroxyl and nightglow intensities, *Planet. Space Sci.*, *20*, 624–627, doi:10.1016/0032-0633(72)90093-1.

Evans, W. F. J., E. J. Llewellyn, and A. Vallance Jones (1973), Altitude distribution of hydroxyl bands of the $\Delta v = 2$ sequence in the nightglow, *Can. J. Phys.*, *51*, 1288–1292, doi:10.1139/p73-170.

French, W. J. R., and F. J. Mulligan (2010), Stability of temperatures from TIMED/SABER v1.07 (2002–2009) and Aura/MLS v2.2 (2004–2009) compared with OH(6-2) temperatures observed at Davis Station, Antarctica, *Atmos. Chem. Phys.*, *10*, 11,439–11,446, doi:10.5194/acp-10-11439-2010.

Gattinger, R. L., A. Vallance Jones, D. A. Degenstein, and E. J. Llewellyn (2010), Quantitative spectroscopy of the aurora. VI. The auroral spectrum from 275 to 815 nm observed by the OSIRIS spectrograph on board the Odin spacecraft, *Can. J. Phys.*, *88*, 559–567, doi:10.1139/P10-037.

Kaufmann, M., C. Lehmann, L. Hoffmann, B. Funke, M. López-Puertas, C. von Savigny, and M. Riese (2008), Chemical heating rates derived from SCIAMACHY vibrationally excited OH limb emission spectra, *Adv. Space Res.*, *41*, 1914–1920, doi:10.1016/j.asr.2007.07.045.

Kovács, I. (1969), *Rotational Structure in the Spectra of Diatomic Molecules*, Adam Hilger Ltd., London, U. K.

Liu, G., and G. G. Shepherd (2006), An empirical model for the altitude of the OH nightglow emission, *Geophys. Res. Lett.*, *33*, L09805, doi:10.1029/2005GL025297.

Llewellyn, E. J., et al. (2004), The OSIRIS instrument on the Odin spacecraft, *Can. J. Phys.*, *82*, 411–422, doi:10.1139/P04-005.

López-Moreno, J. J., R. Rodrigo, F. Moreno, M. López-Puertas, and A. Molina (1987), Altitude distribution of vibrationally excited states of hydroxyl at levels $v = 2$ to $v = 7$, *Planet. Space Sci.*, *35*, 1029–1038, doi:10.1016/0032-0633(87)90007-9.

McDade, I. C. (1991), The altitude dependence of the OH($X\,^2\Pi$) vibrational distribution in the nightglow: Some model expectations, *Planet. Space Sci.*, *39*, 1049–1057, doi:10.1016/0032-0633(91)90112-N.

McDade, I. C., and E. J. Llewellyn (1987), Kinetic parameters related to sources and sinks of vibrationally excited OH in the nightglow, *J. Geophys. Res.*, *92*, 7643–7650, doi:10.1029/JA092iA07p07643.

McDade, I. C., E. J. Llewellyn, D. P. Murtagh, and R. G. H. Greer (1987), Eton 5: Simultaneous rocket measurements of the OH Meinel $\Delta v = 2$ sequence and (8,3) band emission profiles in the nightglow, *Planet. Space Sci.*, *35*, 1137–1147, doi:10.1016/0032-0633(87)90020-1.

Meinel, A. B. (1950), OH emission bands in the spectrum of the night sky. I, *Astrophys. J.*, *111*, 555–564, doi:10.1086/145296.

Mende, S. B., G. R. Swenson, S. P. Geller, R. A. Viereck, E. Murad, and C. P. Pike (1993), Limb view spectrum of the Earth's airglow, *J. Geophys. Res.*, *98*, 19,117–19,125, doi:10.1029/93JA02282.

Mulligan, F. J., and R. P. Lowe (2008), OH-equivalent temperatures derived from ACE-FTS and SABER temperature profiles—A comparison with OH*(3-1) temperatures from Maynooth (53.2°N, 6.4°W), *Ann. Geophys.*, *26*, 795–811, doi:10.5194/angeo-26-795-2008.

Mulligan, F. J., M. E. Dyrland, F. Sigernes, and C. S. Deehr (2009), Inferring hydroxyl layer peak heights from ground-based measurements of OH(6-2) band integrated emission rate at Longyearbyen (78°N, 16°E), *Ann. Geophys.*, *27*, 4197–4205, doi:10.5194/angeo-27-4197-2009.

Murtagh, D., et al. (2002), An overview of the Odin atmospheric mission, *Can. J. Phys.*, *80*, 309–319, doi:10.1139/P01-157.

Picone, J. M., A. E. Hedin, D. P. Drob, and A. C. Aikin (2002), NRL-MSISE-00 empirical model of the atmosphere: Statistical comparisons and scientific issues, *J. Geophys. Res.*, *107*(A12), 1468, doi:10.1029/2002JA009430.

Rodgers, C. D. (2008), *Inverse Methods for Atmospheric Sounding*, World Sci. Co., Singapore.

Rogers, J. W., R. E. Murphy, A. T. Stair Jr., J. C. Ulwick, K. D. Baker, and L. L. Jensen (1973), Rocket-borne radiometric measurements of OH in the auroral zone, *J. Geophys. Res.*, *78*, 7023–7031, doi:10.1029/JC078i030p07023.

Rothman, L. S., et al. (2013), The HITRAN2012 molecular spectroscopic database, *J. Quant. Spectros. Radiat. Transfer*, *130*, 4–50, doi:10.1016/j.jqsrt.2013.07.002.

Sheese, P. E., E. J. Llewellyn, R. L. Gattinger, A. E. Bourassa, D. A. Degenstein, N. D. Lloyd, and I. C. McDade (2010), Temperatures in the upper mesosphere and lower thermosphere from OSIRIS observations of O_2 A-band emission spectra, *Can. J. Phys.*, *88*, 919–925, doi:10.1139/P10-093.

Takahashi, H., C. M. Wrasse, D. Gobbi, T. Nakamura, K. Shiokawa, and L. M. Lima (2005), Airglow OH emission height inferred from OH temperature and meteor trail diffusion coefficient, *Adv. Space Res.*, *35*, 1940–1944, doi:10.1016/j.asr.2005.05.052.

von Savigny, C., and O. Lednyts'kyy (2013), On the relationship between atomic oxygen and vertical shifts between OH Meinel bands originating from different vibrational levels, *Geophys. Res. Lett.*, *40*, 5821–5825, doi:10.1002/2013GL058017.

von Savigny, C., I. C. McDade, K.-U. Eichmann, and J. P. Burrows (2012), On the dependence of the OH* Meinel emission altitude on vibrational level: SCIAMACHY observations and model simulations, *Atmos. Chem. Phys.*, *12*, 8813–8828, doi:10.5194/acp-12-8813-2012.